RBF moment computation and meshless cubature on general polygonal regions [*]

A. Sommariva[1] and M. Vianello
Department of Mathematics, University of Padova, Italy

Abstract

We obtain analytical formulas for the computation of integrals (moments) of all the most common Radial Basis Functions (usually shortened as RBFs) on polygonal regions that may be nonconvex or even multiply connected. With RBFs of finite regularity, such as Thin-Plate Splines, Wendland functions and Radial Powers, our Matlab codes, based on standard linear solvers for the corresponding moment matching systems, provide cubature rules that are reasonably accurate and numerically stable.

2010 AMS subject classification: Primary 65D05; Secondary: 65D32.

Keywords: numerical cubature, scattered data, Radial Basis Functions (RBFs), polygonal regions, Green's formula.

1   Introduction

The main purpose of this paper is to provide cubature rules on polygonal regions Ω of the form

$$\int_{\Omega} f(x,y)dx\,dy \approx \sum_{i=1}^{N} w_k f(x_k, y_k) \tag{1}$$

where the nodes $P_k = (x_k, y_k) \in \Omega$, $k = 1, \ldots, N$, are scattered.

In [15] we coped with the problem in the case $\Omega = [-1, 1]^2$ by RBF (Radial basis Function) interpolation. By means of several RBFs ϕ, we first computed the moments $\gamma_k = \int_\Omega \phi(\|P - P_k\|_2) \, dx \, dy$ and from these they obtained the weights w_k, $k = 1, \ldots, N$, after solving the corresponding moment matching system. The moment computation was based on partitioning the square in some right triangles, recovering analytically the moments over these subdomains without the need of numerical cubature.

Later, in [16], we investigated the more general case of simple polygons Ω, calculating the moments γ_k by a technique based on the application of Gauss-Green theorem in Cartesian coordinates. In particular, if $\phi(r) = r^2 \log(r)$, i.e. a Thin-Plate Spline, we were able again to determine explicitly γ_k. However it is not straightforward to generalize this result to wider families of RBFs.

In [12], after some preliminary papers, the authors explored the case in which Ω is a smooth surface in $\mathbb{R}^3$ with boundaries, with planar regions as particular case. Concerning polygonal regions, the software accompanying that work shows the case of the square $[-1/2, 1/2] \times [-1/2, 1/2]$ as an example.

Here we are interested in a more direct approach, suitable for general polygonal regions on the plane. Differently from [16], we intend to compute the moments of a wide class of RBFs ϕ, including some with compact support, on regions that may be nonconvex or multiply connected or even disconnected as well as multiply intersected polygons. In particular, we consider two different approaches for the computation of γ_k, one that uses the Matlab built-in environment `polyshape` via triangulation and generalises the method used in [15], as well as another one triangulation-free, based on Gauss-Green theorem as in [16], but in polar coordinates. We point out that in both cases, for most of the RBFs no cubature routine is actually required to compute the moments, that on the contrary are obtained analytically.

The paper has the following structure. In Section 2, we briefly recall some basic results about RBF interpolation and cubature on scattered data. In Section 3, we describe the techniques mentioned above to compute the RBF moments γ_k. In Section 4, we test numerically some of these rules on complicated nonconvex polygonal regions with many sides and possible holes. In particular, with Wendland functions, Thin-Plate Splines and Radial Powers we show experimentally that the rules are stable and the moment computation is relatively fast. All the Matlab routines used in our tests are available at [14]. Finally, in the Appendix, we report some primitives obtained analytically to compute γ_k by means of Gauss-Green theorem (in polar coordinates).

2 Preliminaries on RBF cubature

In this section we briefly recall some basic definitions and results that will be useful in the sequel, referring the reader to the relevant monographs [2, 5, 6, 17] for a comprehensive theory and computational issues.

We will denote by $\mathbb{P}_m^d$ the vector space of $d-$variate real valued polynomials of total degree not exceeding m.

A Radial Basis Function $\phi(r) : [0, +\infty) \to \mathbb{R}$, often shortened by the term RBF, is *strictly positive definite* in $\mathbb{R}^d$ (sometimes referred as SPD), if

$$\sum_{j=1}^{N} \sum_{k=1}^{N} c_j c_k \phi(\|P_j - P_k\|_2) \geq 0 \tag{2}$$

for any N pairwise different points $P_1, \ldots, P_N \in \mathbb{R}^d$ and $c_1, \ldots, c_N \in \mathbb{R}$, with the quadratic form (2) null only when $c_1 = \ldots = c_N = 0$.

A key result that suggests its use for interpolation on scattered data is that for any choice of N distinct points $P_1, \ldots, P_N \in \mathbb{R}^d$, setting $\phi_i(P) := \phi(\|P - P_i\|_2)$, there is a unique function

$$s(P) = \sum_{i=1}^{N} c_i \phi_i(P),$$

that interpolates the data $X = \{(P_i, f_i)\}_{i=1,\ldots,N}$, i.e. such that $s(P_i) = f_i$ for $i = 1, \ldots, N$.

More generally a RBF is *strictly conditionally positive of order m* (often shortened as SCPD), if

$$\sum_{j=1}^{N} \sum_{k=1}^{N} c_j c_k \phi(\|P_j - P_k\|_2) \geq 0 \tag{3}$$

holds for any N distinct points $P_1, \ldots, P_N \in \mathbb{R}^d$ and $c_1, \ldots, c_N \in \mathbb{R}$ satisfying

$$\sum_{i=1}^{N} c_i p(P_i) = 0 \tag{4}$$

for any real valued polynomial $p \in \mathbb{P}_{m-1}^d$, with the quadratic form (3) null only when $c_1 = \ldots = c_N = 0$.

Also in this case, it is well-known that there exists a unique function $s(P)$ of the form

$$s(P) = \sum_{i=1,\ldots,N} c_i \phi_i(P) + \pi(P), \ \pi \in \mathbb{P}_{m-1}^d \tag{5}$$

3

that interpolates the data $X = \{(P_i, f_i)\}_{i=1,...,N}$. To simplify the notation, we may think to strictly positive definite RBF as strictly conditionally positive of order 0, i.e. in which there is not the constraint (4) on the coefficients and that $\pi \equiv 0$ in (5).

During the years, many RBFs have been discovered. The most common ones, used in bivariate settings, are the following

RBF	$\phi(r)$	order
Multiquadric	$\sqrt{1 + r^2}$	1
Thin-Plate Spline	$r^2 \log(r)$	2
Inverse Multiquadric	$\frac{1}{1+r^2}$	0
Wendland W2	$(1 + 4r) \cdot (\max(0, (1 - r)))^4$	0
Gaussian	$\exp(-r^2)$	0
Radial Powers	$r^\beta, \beta \notin 2\mathbb{N}$	$m = \lceil \beta/2 \rceil$,

but a comprehensive list should take into account also other families as Laguerre-Gaussians, Matérn, Poisson radial functions, Generalized Inverse Multiquadrics, see [5, p.38], [17], as well as other compactly supported RBFs, see e.g. [2, p.147], [5, p.85], [17, p.129]. Furthermore, for many of these RBFs one often considers their scaled counterpart

$$\phi_\epsilon(r) = \phi(\epsilon r) \ ,$$

the determination of a (near) optimal "shape parameter" $\epsilon > 0$ being a difficult issue; cf., e.g., [3, 4, 7, 8, 9] with the references therein.

Let us suppose that ϕ is SCPD of order m on Ω. A *direct* approach for determining the interpolation coefficients $\{c_i\}_{i=1,...,N}$ consists first in evaluating the *interpolation matrix*

$$\mathcal{A} := \begin{bmatrix} A & B \\ B^T & 0_{M \times M} \end{bmatrix} \text{ where } A_{i,j} = \phi(\|P_i - P_j\|), B_{i,k} = \pi_k(P_i),$$

where $\{\pi_k\}_{k=1,...,M}$ is a basis of $\mathbb{P}_{m-1}^d$ (in the particular case of strictly positive definite RBF one simply has $\mathcal{A} = A$), and then in solving the square linear system

$$\mathcal{A}\mathbf{C} = \mathbf{F} \text{ where } \mathbf{C} = [\mathbf{c}, \mathbf{d}]^T, \mathbf{F} = [\mathbf{f}, \mathbf{0}]^T, \tag{6}$$

in which $\mathbf{c} = (c_i)_{i=1,...,N}$, $\mathbf{d} = (d_i)_{i=1,...,M}$ are the coefficients of the polynomial π w.r.t. the basis $\{\pi_k\}_{k=1,...,M}$, $\mathbf{f} = (f_i)_{i=1,...,N}$ and $\mathbf{0} \in \mathbb{R}^M$ is the null vector.

Concerning the numerical cubature of a continuous function $f : \Omega \subset \mathbb{R}^d$ on scattered points $\{P_i\}_{i=1,\ldots,N}$ in a compact domain $\Omega \subset \mathbb{R}^d$, the integration of the RBF interpolant s of the couples $(P_i, f(P_i))$ for $i = 1, \ldots, N$ gives

$$I(f) := \int_\Omega f(P)dP \approx I(s) := \int_\Omega s(P)dP = \sum_{i=1}^N c_i \int_\Omega \phi_i(P)dP + \int_\Omega \pi(P)dP.$$

Setting $\mathbf{I}_R = (I(\phi_i))_i$, $\mathbf{I}_\pi = (I(\pi_i))_i$, one obtains

$$I(s) = \langle \mathbf{C}, \mathbf{I} \rangle, \ \text{with} \ \mathbf{C} = [\mathbf{c}, \mathbf{d}]^T, \mathbf{I} = [\mathbf{I}_R, \mathbf{I}_\pi]^T,$$

where $\langle \cdot, \cdot \rangle$ denotes the scalar product in the corresponding dimension. From (6) we have that $\mathbf{C} = \mathcal{A}^{-1}\mathbf{F}$, necessarily if $\mathbf{W} := \mathcal{A}^{-1}\mathbf{I} = [\mathbf{w}, \mathbf{z}]^T$ with $\mathbf{w} \in \mathbb{R}^N$, since $\mathcal{A}$ is symmetric and $\mathbf{F} = [\mathbf{f}, \mathbf{0}]^T$,

$$I(s) = \langle \mathbf{C}, \mathbf{I} \rangle = \langle \mathcal{A}^{-1}\mathbf{F}, \mathbf{I} \rangle = \langle \mathcal{A}^{-1}\mathbf{I}, \mathbf{F} \rangle = \langle \mathbf{W}, \mathbf{F} \rangle = \langle \mathbf{w}, \mathbf{f} \rangle = \sum_{i=1}^N w_i f_i. \quad (7)$$

In other words, one solves the square linear system

$$\mathcal{A}\,\mathbf{W} = \mathbf{I}, \ \ \mathbf{W} = \begin{bmatrix} \mathbf{w} \\ \mathbf{z} \end{bmatrix} \quad \text{(moment matching system)} \quad\quad (8)$$

and determines the weights by extracting the first N components $\mathbf{w}$ of the solution $\mathbf{W}$.

Following [15, 16], we recall a basic cubature error estimate, concerning convergence and stability with respect to different perturbations arising from moment approximation as well as possible noise in the functional data. In this estimate two key parameters in RBF interpolation/cubature error analysis appear, namely the *fill distance*

$$h = \max_{P \in \Omega} \min_{1 \leq i \leq n} |P - P_i|$$

and the *separation distance*

$$q = \min_{j \neq i} \{|P_j - P_i|\} \leq 2h.$$

Below we denote by $\tilde{\mathbf{I}} \approx \mathbf{I}$ the approximate RBF moments, by $\tilde{\mathbf{W}}$ and $\tilde{\mathbf{w}}$ the corresponding perturbed weights and by $\tilde{\mathbf{f}} \approx \mathbf{f}$ the noisy functional data. The following estimate holds for the overall error of the perturbed cubature formula $\langle \tilde{\mathbf{w}}, \tilde{\mathbf{f}} \rangle$

$$|I(f) - \langle \tilde{\mathbf{w}}, \tilde{\mathbf{f}} \rangle| \leq |I(f) - I(s)| + |\langle \mathbf{W} - \tilde{\mathbf{W}}, \mathbf{F} \rangle| + |\langle \tilde{\mathbf{W}}, \mathbf{F} - \tilde{\mathbf{F}} \rangle|$$

$$\leq \sqrt{area(\Omega)} \, \|f - s\|_{L^2(\Omega)} + \|\mathcal{A}^{-1}\|_2 \, \|\mathbf{f}\|_2 \, \|\mathbf{I} - \tilde{\mathbf{I}}\|_2 + \|\tilde{\mathbf{w}}\|_1 \, \|\mathbf{f} - \tilde{\mathbf{f}}\|_\infty$$

$$= \mathcal{O}\left(\alpha(h)\right) + \mathcal{O}\left(\frac{1}{\lambda(q)}\right) \, \|\mathbf{I} - \tilde{\mathbf{I}}\|_2 + \|\mathbf{f} - \tilde{\mathbf{f}}\|_\infty \sum_{i=1}^{N} |\tilde{w}_i| \,, \qquad (9)$$

where $\alpha(h) \downarrow 0$ as $h \to 0$ and $\lambda(q) \downarrow 0$ as $q \to 0$ (and thus as $h \to 0$), $\lambda(q)$ being the minimimal eigenvalue of $\mathcal{A}$, see [2, 17] (in the SPD case, (9) holds again with small substituting capital letters, and A substituting $\mathcal{A}$).

In (9) one can clearly see an occurrence of the "*uncertainty principle*" in RBF interpolation, so summarized in the seminal paper [13]: "*There is no case known where the errors and the sensitivity are both reasonably small*". Here sensitivity refers to the interpolation coefficients or in the present context to the cubature weights, since both are solution of a linear system with the same (symmetric) positive definite matrix, the reciprocal of whose minimal eigenvalue measures in some sense the response to perturbations of the right-hand side. In particular, for C^∞ RBFs, such as Gaussians and (inverse) multiquadrics, the infinitesimal rates of $\alpha(h)$ and $\lambda(q)$ are both *exponential*, while for RBFs of finite regularity, like such as TPS or Wendland functions, the rates are both *algebraic*. On the other hand, as usual in cubature settings the response to errors in the functional data is measured by the 1-norm of the computed weights (that are in general not all positive).

In the present paper, we focalize on RBFs of finite regularity, where the cubature rules obtained by direct solvers of the moment matching system turn out to be reasonably accurate and numerically stable (for not too dense data sites), concerning both, the effect of errors on the moments and noise on the functional data. Nevertheless, we have chosen to give also the analytical formulas for the computation of moments of C^∞ RBFs, since any available method to cope the system sensitivity in the computation of the interpolation coefficients could be immediately transferred to the computation of the cubature weights.

3   RBF moment computation

In this section we study the moment computation of a large class of RBFs in the case $\Omega \subset \mathbb{R}^2$ is a *polygonal region*. With this term we intend that Ω has polygonal boundaries, also considering the case of domains that are multiply connected (i.e. the domain Ω may contain holes whose boundaries are polygons). Furthermore, Ω may not be a connected domain.

We will consider two different approaches, one that uses the Matlab built-in environment `polyshape` and generalises the method used in [15] as

well as another one based on Gauss-Green theorem, as in [16], but in polar coordinates.

3.1 Triangulation-based moment computation

Given a polygonal domain Ω, not necessarily simply connected or connected, the Matlab environment `polyshape` [11] determines a triangulation $\Delta = \mathcal{T}_{i=1,\dots,l}$ of Ω. In the case of *not self intersecting* polygons with L sides, there is numerical evidence that Δ is minimal, which means that the cardinality l of Δ is equal to $L - 2$ (see [1] for additional details about the triangulation as well as algebraic cubature on such regions).

In view of the additivity of the integral operator, considering for sake of generality the scaled RBF case in which

$$\phi_{k,\epsilon}(P) = \phi(\epsilon \, \|P - P_k\|_2) \, ,$$

$$
\begin{aligned}
I_\Omega(\phi_{k,\epsilon}) \; &:= \; \int_\Omega \phi(\epsilon \, \|P - P_k\|_2) \, dx \, dy \\
&= \; \sum_{i=1}^l \int_{\mathcal{T}_i} \phi(\epsilon \, \|P - P_k\|_2) \, dx \, dy = \sum_{i=1}^l I_{\mathcal{T}_i}(\phi_{k,\epsilon})
\end{aligned}
$$

and thus it is sufficient to determine each $I_{\mathcal{T}_i}(\phi_{k,\epsilon})$ to get $I_\Omega(\phi_{k,\epsilon})$. In view of this observation, we focus our attention on the computation of the moment of each $\phi_{k,\epsilon}$ on a triangle $\mathcal{T}$ with vertices A, B, C, ordered counterclockwise.

In [15] we investigated RBF cubature on a square Ω. The key point was the computation of $I_\Omega(\phi_k)$ for $k = 1, \dots, N$. In particular, we partitioned the domain in right triangles $\mathcal{T}_{P_k}^\perp$, having the center P_k as one the vertices, and computed the moments in any right triangle of such kind.

Let $\mathcal{T}_{P_k,M,H}^\perp$ be a triangle, with the angle $\theta^* := H\hat{P}_k M$ and $M\hat{H}P_k = \pi/2$ (see Figure 1). Next, set r_0, r_1 respectively the length of the segments $\overline{P_k H}$ and $\overline{P_k M}$. By basic trigonometric equalities, $\theta^* = \arccos\left(\frac{r_0}{r_1}\right)$.

Then,

$$
\begin{aligned}
I_{\mathcal{T}_{P_k,M,H}^\perp}(\phi_{k,\epsilon}) \; &= \; \int_{\mathcal{T}_{P_k,M,H}^\perp} \phi\left(\epsilon \, \|P - P_k\|_2\right) dx \, dy \\
&= \; \int_0^{\theta^*} \int_0^{r_0/\cos(\theta)} \phi(\epsilon \, r) r \, dr \, d\theta = \epsilon^{-2} \int_0^{\theta^*} \Psi\left(\frac{\epsilon \, r}{\cos(\theta)}\right) d\theta
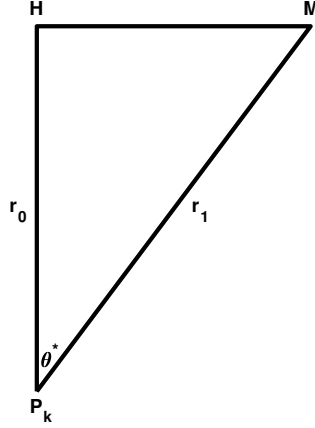\end{aligned}
$$

7

Figure 1: A right triangle $\mathcal{T}^{\perp}_{P_k,M,H}$.

where

$$\Psi(\rho) := \int_0^{\rho} \phi(r)r\,dr. \tag{10}$$

In [15] we determined Ψ for a wide class of RBFs and explicit formulas of $I_{\mathcal{T}^{\perp}_{P_k,M,H}}(\phi_{k,\epsilon})$ for Thin-Plate Splines, Multiquadrics, Inverse Multiquadrics and Wendland W2. We are here able to apply this technique also to Radial Powers, Gaussians and other Wendland functions such as W0, W4, W6. Unfortunately, the corresponding formulas are too long to be included in this paper, and can be found in the Matlab codes available at [14].

Here, first we show how to compute each $I_{\mathcal{T}}(\phi_{k,\epsilon})$ when the triangle $\mathcal{T}$ has vertices $A = P_k$, B, C, and then apply this result in the general case in which A may not coincide with P_k. In our analysis we suppose that all the triangles are not degenerate, otherwise $I_{\mathcal{T}}(\phi_{k,\epsilon}) = 0$.

So let $\mathcal{T}_{A,B,C}$ be a non degenerate triangle with vertices $A = P_k$, B, C, oriented counterclockwise (see Figure 2). If the projection H of P_k on the straight line containing the segment $\overline{BC}$

- belongs to $\overline{BC}$, then $\mathcal{T}_{P_k,B,C}$ can be partitioned in the right triangles $\mathcal{T}^{\perp}_{P_k,B,H}$, $\mathcal{T}^{\perp}_{P_k,H,C}$, hence

$$I_{\mathcal{T}_{P_k,B,C}}(\phi_{k,\epsilon}) = I_{\mathcal{T}^{\perp}_{P_k,B,H}}(\phi_{k,\epsilon}) + I_{\mathcal{T}^{\perp}_{P_k,H,C}}(\phi_{k,\epsilon})$$

  where $\mathcal{T}^{\perp}_{P_k,B,H}(\phi_{k,\epsilon})$, $\mathcal{T}^{\perp}_{P_k,H,C}(\phi_{k,\epsilon})$ are right triangles with a vertex in the center and the moments of $\phi_{k,\epsilon}$ in these subdomains can be computed using the techniques suggested in [15];
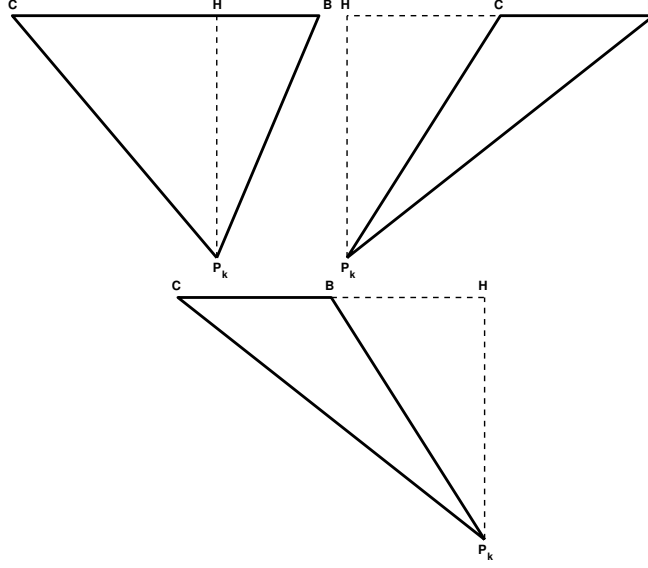
8

Figure 2: Triangles $\mathcal{T}_{P_k,B,C}$ and their partitioning into right triangles.

- is on the left of C, then the triangle $\mathcal{T}_{P_k,B,C}$ is the set difference (here and below set differences are intended up to zero measure subsets that are the sides) of the right triangles $\mathcal{T}^{\perp}_{P_k,C,H}$, $\mathcal{T}^{\perp}_{P_k,B,H}$, with $\mathcal{T}^{\perp}_{P_k,C,H} \subseteq \mathcal{T}^{\perp}_{P_k,B,H}$ and consequently

$$I_{\mathcal{T}_{P_k,B,C}}(\phi_{k,\epsilon}) = I_{\mathcal{T}^{\perp}_{P_k,B,H}}(\phi_{k,\epsilon}) - I_{\mathcal{T}^{\perp}_{P_k,C,H}}(\phi_{k,\epsilon})$$

where the integrals on the right hand side can be computed as in [15];

- is on the right of B, then the triangle $\mathcal{T}_{P_k,B,C}$ is the set difference of the right triangles $\mathcal{T}^{\perp}_{P_k,H,C}$, $\mathcal{T}^{\perp}_{P_k,B,H}$, with $\mathcal{T}^{\perp}_{P_k,B,H} \subseteq \mathcal{T}^{\perp}_{P_k,H,C}$ and consequently

$$I_{\mathcal{T}_{P_k,B,C}}(\phi_{k,\epsilon}) = I_{\mathcal{T}^{\perp}_{P_k,H,C}}(\phi_{k,\epsilon}) - I_{\mathcal{T}^{\perp}_{P_k,B,H}}(\phi_{k,\epsilon})$$

and again the integrals on the right hand side can be determined as in [15].

Now, being able to compute integrals of the form $I_{\mathcal{T}_{P_k,B,C}}(\phi_{k,\epsilon})$, we intend to compute the moment of $\phi_{k,\epsilon}$ on a general triangle $\mathcal{T}_{A,B,C}$. Again many cases may arise (see Figure 3):
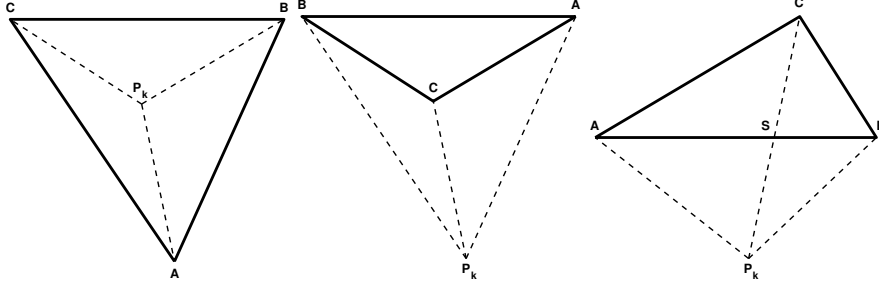
Figure 3: Triangles $\mathcal{T}_{A,B,C}$, the RBF center P_k and partitioning into triangles having P_k as vertex.

- if $P_k \in \mathcal{T}_{A,B,C}$ then the triangle $\mathcal{T}_{A,B,C}$ can be partitioned in $\mathcal{T}_{P_k,A,B}$, $\mathcal{T}_{P_k,B,C}$, $\mathcal{T}_{P_k,C,A}$ and thus

$$I_{\mathcal{T}_{A,B,C}}(\phi_{k,\epsilon}) = I_{\mathcal{T}_{P_k,A,B}}(\phi_{k,\epsilon}) + I_{\mathcal{T}_{P_k,B,C}}(\phi_{k,\epsilon}) + I_{\mathcal{T}_{P_k,C,A}}(\phi_{k,\epsilon}),$$

  where all the triangles involved in the r.h.s. have P_k as one of the vertices;

- if $P_k \notin \mathcal{T}_{A,B,C}$ and the intersection of each segment $\overline{P_k A}$, $\overline{P_k B}$, $\overline{P_k C}$ with the interior of the triangle $\mathcal{T}_{A,B,C}$ is empty then the convex-hull of the points P_k, A, B, C, is a triangle with P_k as one of the vertices, say $\mathcal{T}_{P_k,A,B}$; since C belongs to the interior of this triangle then $\mathcal{T}_{P_k,A,B}$ can be partitioned into $\mathcal{T}_{P_k,A,C}$, $\mathcal{T}_{P_k,C,B}$ and $\mathcal{T}_{A,B,C}$, and consequently

$$I_{\mathcal{T}_{A,B,C}}(\phi_{k,\epsilon}) = I_{\mathcal{T}_{P_k,A,B}}(\phi_{k,\epsilon}) - I_{\mathcal{T}_{P_k,A,C}}(\phi_{k,\epsilon}) - I_{\mathcal{T}_{P_k,C,B}}(\phi_{k,\epsilon});$$

  where all the triangles involved in the r.h.s. have P_k as one of the vertices;

- if $P_k \notin \mathcal{T}_{A,B,C}$ and the intersection of each segment $\overline{P_k A}$, $\overline{P_k B}$, $\overline{P_k C}$ with the interior of the triangle $\mathcal{T}_{A,B,C}$ is not empty then there is only one segment for which this happens, say $P_k C$; in this case let S be the intersection of the segment $\overline{AB}$ with $\overline{P_k C}$ and observe that the quadrangle with vertices A, P_k, B, C, can be partitioned by $\mathcal{T}_{P_k,C,A}$ and $\mathcal{T}_{P_k,B,C}$ as well as by $\mathcal{T}_{A,B,C}$, $\mathcal{T}_{P_k,S,A}$, $\mathcal{T}_{P_k,B,S}$, from which we have

$$I_{\mathcal{T}_{P_k,C,A}}(\phi_{k,\epsilon}) + I_{\mathcal{T}_{P_k,B,C}}(\phi_{k,\epsilon}) = I_{\mathcal{T}_{A,B,C}}(\phi_{k,\epsilon}) + I_{\mathcal{T}_{P_k,S,A}}(\phi_{k,\epsilon}) + I_{\mathcal{T}_{P_k,B,S}}(\phi_{k,\epsilon})$$

  and thus

$$I_{\mathcal{T}_{A,B,C}}(\phi_{k,\epsilon}) = I_{\mathcal{T}_{P_k,C,A}}(\phi_{k,\epsilon}) + I_{\mathcal{T}_{P_k,B,C}}(\phi_{k,\epsilon}) - \left(I_{\mathcal{T}_{P_k,S,A}}(\phi_{k,\epsilon}) + I_{\mathcal{T}_{P_k,B,S}}(\phi_{k,\epsilon}) \right).$$

10

where all the triangles involved in the r.h.s. have P_k as one of the vertices.

In all the possible cases, we have reduced our analysis in computing the moments over triangles with P_k as one of the vertices and we can apply to each of them the strategy previously introduced.

At this point, we are able to integrate the scaled RBF $\phi_{k,\epsilon}$ on each possible triangle and thus, by additivity, also on the polygonal domain.

We succeeded in applying these techniques to multiquadrics, inverse multiquadrics, Thin-Plate Splines, radial splines of the form $\phi(r) = r^k$ with $k = 3, 5, 7$, RBFs with compact support such as $W0$, $W2$, $W4$, $W6$ (see [5, p.88]). In the case of the Gaussian radial basis the code requires the evaluation of the Owen's T-function, a non trivial task that needs the numerical computation of definite integrals.

3.2 Triangulation-free moment computation

In [16], we computed $I(\phi_{k,\epsilon})$ by Gauss-Green formula, where ϕ is a Thin-Plate Splines and Ω is a polygon. In particular, since interpolation by such RBF does not depend on ϵ, we took into account only the case $\epsilon = 1$, i.e. $\phi_{k,1} = \phi_k$. The key idea was that by Gauss-Green theorem, representing the moment problem in Cartesian coordinates,

$$I_\Omega(\phi_k) = \int_\Omega \phi(\|P - P_k\|_2)dP = \oint_{\partial\Omega} \left(\int \phi(\|P - P_k\|_2)dx \right) dy, \ P = (x, y).$$

As first result, we were able to compute an explicit primitive

$$\Phi_k(P) = \int \phi(\|P - P_k\|_2)dx.$$

Then, if the boundary $\partial\Omega$ of the simple polygon Ω. i.e. without self-intersections, has vertices V_j, $j = 1, \ldots, n + 1$ (ordered counterclockwise), with $V_{n+1} = V_1$, denoting by $\overline{V_j V_{j+1}}$ the segment connecting V_j with V_{j+1}, we observed that

$$\oint_{\partial\Omega} \left(\int \phi(\|P - P_k\|_2)dx \right) dy = \oint_{\partial\Omega} \Phi_k(P)dy = \sum_{j=1}^{n} \int_{\overline{V_j V_{j+1}}} \Phi_k(P)dy.$$

Finally we computed explicitly each $I_{\overline{V_j V_{j+1}}}(\phi_k) = \int_{\overline{V_j V_{j+1}}} \Phi_k(P)dy$.

Though this approach worked well for Thin-Plate Splines, we were not able to determine closed formulas of the integrals $I_{\overline{V_j V_{j+1}}}(\phi_k)$ for a wider class of RBFs.

The purpose of this section is to introduce a strategy that partially fills this gap, representing this time the moment problem in polar coordinates, and using again the Gauss-Green theorem. In our analysis, the function $\phi \in C([0, +\infty))$ is not necessarily a TPS.

Setting $r = \|P - P_k\|_2$ and being $\phi_{k,\epsilon}(P) = \phi(\epsilon \|P - P_k\|_2)$, we have

$$
\begin{aligned}
I_\Omega(\phi_{k,\,\epsilon}) \quad &:= \quad \int_\Omega \phi(\epsilon \|P - P_k\|_2) dP = \oint_{\partial\Omega} \left(\int r\phi(\epsilon\, r) dr \right) d\theta \\
&= \quad \sum_{j=1}^n \int_{\overline{V_j V_{j+1}}} \int r\phi(\epsilon\, r) dr \; d\theta.
\end{aligned}
\tag{11}
$$

Now we intend to compute each term $\int_{\overline{V_j V_{j+1}}} \int r\phi(\epsilon\, r) dr \, d\theta$ of the sum in (11) and show how it is somehow connected to the triangle $\mathcal{T}_{P_k, V_j, V_{j+1}}$.
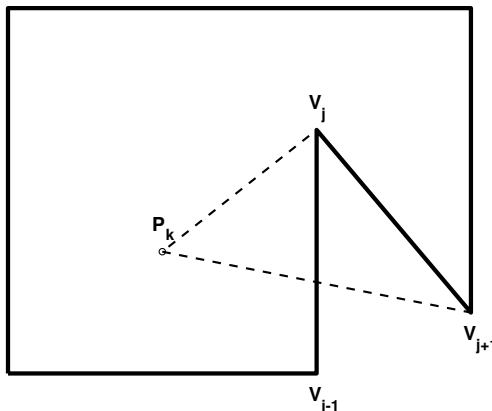

Figure 4: Example of a polygon with vertices ordered counterclockwise, but with a local triangle $\mathcal{T}_{P_k, V_j, V_{j+1}}$ with vertices ordered clockwise.

We will suppose that $\mathcal{T}_{P_k, V_j, V_{j+1}}$ is not degenerate (otherwise the analysis becomes trivial) and has vertices ordered counterclockwise.

We also observe that it may happen that though the polygon vertices are ordered counterclockwise, the triangle $\mathcal{T}_{P_k, V_j, V_{j+1}}$ is ordered clockwise (see Figure 4). In this case one must apply the procedure that we will describe below, changing finally sign to the obtained value.

Let r_0 be the length of the segment $\overline{P_k V_j}$, θ_0 the angle $P_k \hat{V}_j V_{j+1}$, θ^* the angle $V_j \hat{P}_k V_{j+1}$ (see Figure 5).
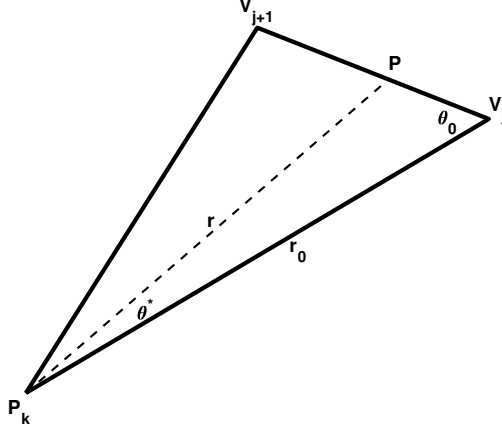
Figure 5: The triangle $\mathcal{T}_{P_k,V_j,V_{j+1}}$ with vertices ordered counterclockwise.

Setting $r^*(\theta) = r_0 \sin(\theta_0)/\sin(\theta_0 + \theta)$, $t = \epsilon\, r$ and $s = \theta_0 + \theta$, we have

$$
\begin{aligned}
\int_{\overline{V_j V_{j+1}}}\int r\phi(\epsilon\, r)dr\; d\theta &= \int_0^{\theta^*}\int_0^{r^*(\theta)} \phi(\epsilon\, r)drd\theta \\
&= \int_0^{\theta^*}\int_0^{r_0 \sin(\theta_0)/\sin(\theta_0+\theta)} r\phi(\epsilon\, r)drd\theta \\
&= \epsilon^{-2}\int_0^{\theta^*}\int_0^{\epsilon\, r_0 \sin(\theta_0)/\sin(\theta_0+\theta)} t\phi(t)dtd\theta \\
&= \epsilon^{-2}\int_{\theta_0}^{\theta^*+\theta_0}\int_0^{\epsilon\, r_0 \sin(\theta_0)/\sin(s)} t\phi(t)dt\, ds.
\end{aligned}
$$

Thus, if $\Psi(\rho) := \int_0^\rho t\phi(t)dt$, $c_{\theta_0,\epsilon} := \epsilon\, r_0 \sin(\theta_0)$, being $\Psi(0) = 0$, by the fundamental theorem of calculus

$$
\begin{aligned}
\int_{\overline{V_j V_{j+1}}}\int r\phi(\epsilon\, r)dr\; d\theta &= \epsilon^{-2}\int_{\theta_0}^{\theta^*+\theta_0}\Psi\left(\frac{\epsilon\, r_0 \sin(\theta_0)}{\sin(s)}\right)ds \\
&= \epsilon^{-2}\int_{\theta_0}^{\theta^*+\theta_0}\Psi(c_{\theta_0,\epsilon}/\sin(s))\, ds. \qquad (12)
\end{aligned}
$$

Since we suppose that the triangle $\mathcal{T}_{P_k,V_j,V_{j+1}}$ is not degenerate, $\theta_0 > 0$ is the angle $P_k \hat{V}_j V_{j+1}$, $\theta^* > 0$ is the angle $V_j \hat{P}_k V_{j+1}$, by simple geometric considerations we have that $0 < \theta_0 < \theta_1 := \theta^* + \theta_0 < \pi$ and $c_{\theta_0,\epsilon} = \epsilon\, r_0 \sin(\theta_0) > 0$ (see Figure 5).

13

Hence, the quantity of the r.h.s. of (12) is easily at hand as soon as we are able to compute

$$I_{c,\theta_0,\theta_1}(\Psi) := \int_{\theta_0}^{\theta_1} \Psi(c/\sin(s))\,ds$$

with $0 < \theta_0 < \theta_1 < \pi$ and $c > 0$. Since

$$\int_{\theta_0}^{\theta_1} \Psi(c/\sin(s))\,ds = \int_{\pi/2}^{\theta_1} \Psi(c/\sin(s))\,ds - \int_{\pi/2}^{\theta_0} \Psi(c/\sin(s))\,ds$$

we will restrict our attention to the computation of

$$I_{c,\pi/2,t^*}(\Psi) = \int_{\pi/2}^{t^*} \Psi(c/\sin(s))\,ds, \ \ t^* \in (0,\pi).$$

For many RBFs, symbolic computations by Wolfram Alpha [18] allow an explicit formulation of $I_{c,\pi/2,t^*}(\Psi)$. We achieved this goal for Multiquadrics, Inverse Multiquadrics, Thin-Plate Splines, Radial Powers of the form $\phi(r) = r^k$ with $k = 3, 5, 7$, RBFs with compact support such as $W0$, $W2$, $W4$, $W6$ (see [5, p.88]). For the Gaussian radial function and the Matérn RBFs $\phi(r) = \exp(-r)$ and $\phi(r) = (1+r)\exp(-r)$, we were only able to determine Ψ and computing the required integrals by suitable shifted Gauss-Legendre rules.

In general the explicit formulation of $I_{c,\pi/2,t^*}(\Psi)$ has a very long expression, and for many RBFs can be found in the Appendix of this work, as well as in our Matlab implementation, available at [14].

In most of the cases, as soon as a primitive of $\Psi(c/\sin(s))$ is available, the integral $I_{c,\pi/2,\theta^*}(\Psi)$ can be computed by applying the fundamental theorem of calculus, but in the case of compactly supported RBFs the strategy to use is less direct.

As example, we show what we obtained for the Wendland compactly supported RBF,

$$\phi(r) = (1 + 4r) \cdot (1 - r)_+^4, \text{ where } r_+ = \max(0, r). \tag{13}$$

that is SPD in $\mathbb{R}^d$ for $d \leq 3$ and belonging to $C^2([0, +\infty))$.

Setting

$$\psi(r) := \frac{r^2(8r^5 - 35r^4 + 56r^3 - 35r^2 + 7)}{14},$$

one can see that

$$\psi(\rho) = \int_0^\rho r(1 + 4r) \cdot (1 - r)^4 dt$$

(notice that the integrand is not compactly supported).

Since $[0,1]$ is the support of ϕ, if $\rho \in [0,1]$ then

$$\Psi(\rho) = \int_0^\rho r(1+4r) \cdot (1-r)_+^4 dt = \int_0^\rho r(1+4r) \cdot (1-r)^4 dt = \psi(\rho),$$

while if $\rho > 1$ then

$$\Psi(\rho) = \int_0^\rho t\phi(t)dt = \int_0^1 t\phi(t)dt + \int_1^\rho t\phi(t)dt = \int_0^1 t\phi(t)dt = \psi(1).$$

Consequently we have

$$\Psi(\rho) = \int_0^\rho t\phi(t)dt = \begin{cases} \psi(\rho) & \text{if } \rho \in [0,1] \\ \psi(1) & \text{if } \rho > 1. \end{cases} \tag{14}$$

In particular, one can check by symbolic calculus (e.g. [18]) that the function

$$\begin{aligned}
\mathcal{P}_c^*(s) = & -\frac{1}{672}c^7 \csc^6(s/2) - \frac{1}{112}c^7 \csc^4(s/2) - \frac{5}{112}c^7 \csc^2(s/2) + \\
& \frac{1}{672}c^7 \sec^6(s/2) + \frac{1}{112}c^7 \sec^4(s/2) + \frac{5}{112}c^7 \sec^2(s/2) + \\
& \frac{5}{28}c^7 \log(\sin(s/2)) - \frac{5}{28}c^7 \log(\cos(s/2)) + \frac{4}{3}c^6 \cot(s) + \\
& \frac{1}{2}c^6 \cot(s) \csc^4(s) + \frac{2}{3}c^6 \cot(s) \csc^2(s) - \frac{1}{16}c^5 \csc^4(s/2) - \\
& \frac{3}{8}c^5 \csc^2(s/2) + \frac{1}{16}c^5 \sec^4(s/2) + \frac{3}{8}c^5 \sec^2(s/2) + \frac{3}{2}c^5 \log(\sin(s/2)) - \\
& \frac{3}{2}c^5 \log(\cos(s/2)) + \frac{5}{3}c^4 \cot(s) + \frac{5}{6}c^4 \cot(s) \csc^2(s) - \frac{1}{2}c^2 \cot(s)
\end{aligned} \tag{15}$$

is a primitive of $\psi(c/\sin(t))$.

We are ready to compute

$$I_{c,\pi/2,t^*}(\Psi) = \int_{\pi/2}^{t^*} \Psi(c/\sin(s)) \, ds,$$

with $t^* \in (0, \pi)$.

If $c < 1$ and $c/\sin(t^*) < 1$ then by the monotonicity of $c/\sin(s)$, for any $s \in [\min(\pi/2, t^*), \max(\pi/2, t^*)]$, we have

$$\max_{s\in[\min(\pi/2,t^*),\max(\pi/2,t^*)]} c/\sin(s) = c/\sin(t^*) < 1$$

15

hence by (14) that $\Psi(c/\sin(s)) = \psi(c/\sin(s))$. Thus by the fundamental theorem of calculus, being $\mathcal{P}_c^*(t)$ a primitive of $\psi(c/\sin(t))$,

$$
\begin{aligned}
I_{c,\pi/2,t^*}(\Psi) &:= \int_{\pi/2}^{t^*} \Psi(c/\sin(s))\,ds = \int_{\pi/2}^{t^*} \psi(c/\sin(s))\,ds \\
&= \mathcal{P}_c^*(t^*) - \mathcal{P}_c^*(\pi/2).
\end{aligned} \tag{16}
$$

If $c < 1$ but $c/\sin(t^*) \geq 1$, setting

$$
\tilde{t} := \begin{cases} \arcsin(c), & \text{if } t^* < \pi/2 \\ \pi - \arcsin(c), & \text{if } t^* \geq \pi/2 \end{cases}
$$

we have that

$$
\begin{cases} c/\sin(s) \leq 1, & \text{for } s \in [\min(\pi/2,\tilde{t}), \max(\pi/2,\tilde{t})] \\[2mm] c/\sin(s) \geq 1, & \text{otherwise.} \end{cases} \tag{17}
$$

Thus by (14)

$$
\Psi(c/\sin(s)) = \begin{cases} \psi(c/\sin(s)), & \text{if } s \in [\min(\pi/2,\tilde{t}), \max(\pi/2,\tilde{t})] \\ \psi(1), & \text{otherwise.} \end{cases}
$$

Hence,

$$
\begin{aligned}
I_{c,\pi/2,t^*}(\Psi) &:= \int_{\pi/2}^{t^*} \Psi(c/\sin(s))\,ds = \int_{\pi/2}^{\tilde{t}} \psi(c/\sin(s))\,ds + \int_{\tilde{t}}^{t^*} \psi(c/\sin(s))\,ds \\
&= \mathcal{P}_c^*(\tilde{t}) - \mathcal{P}_c^*(\pi/2) + (t^* - \tilde{t})\psi(1).
\end{aligned} \tag{18}
$$

Finally, if $c \geq 1$ then $c/\sin(t) \geq 1$ for any $t \in (0,\pi)$, implying that $\Psi(c/\sin(t)) = \psi(1)$ and thus

$$
I_{c,\pi/2,t^*}(\Psi) := \int_{\pi/2}^{t^*} \Psi(c/\sin(s))\,ds = (t^* - \pi/2)\psi(1). \tag{19}
$$

Consequently, in the case of Wendland functions (13), the moments $I_\Omega(\phi_{i,\epsilon})$ can be computed without resorting to numerical adaptive cubature. The same strategy can be applied more generally to RBFs having $[0,1]$ as support, as soon as the function Ψ is available. The generalization to more general supports $[0, \epsilon^{-1}]$ is a consequence of (12).

Remark. If the polygonal domain Ω is not simply connected, one applies this technique to all the polygonal boundaries, multiplying by -1 the contributions obtained on the holes of each connected component.

4 Numerical examples

In this section we test our meshless cubature rules by RBFs, using the methods introduced above. As domains Ω, we consider a nine sides nonconvex polygon Ω_1 and a complicated disconnected polygonal region Ω_2 with two holes and an internal "island", see Figure 6).

First we compare the cputimes of the two approaches (triangulation-based and triangulation-free) for computing the moments

$$\gamma_k = \int_{\Omega_s} \phi(\|P - P_k\|_2)\,dxdy, \ \ P_k \in \Omega_s, \ k = 1, \ldots, N$$

and then we perform numerical cubature over these domains, showing the quality of the integration by several RBFs.

As functions ϕ in the moment computation step, we consider both, C^∞ RBFs such as Multiquadrics (MQ), Gaussians (G), Inverse Multiquadrics (IMQ), and RBFs of finite regularity such as Wendland W2, Thin-Plate Splines (TPS) and Radial Powers $\phi(r) = r^3$ (RP). As for the shape parameter, we set $\epsilon = 1$.

We perform a battery of tests, on both the regions Ω_s, comparing the results with those obtained by the algebraic cubature routines introduced in [1], with algebraic degree of precision $ADE = 1000$. In Tables 1, 2 we report the worst absolute and relative error in computing the RBF moments, as well as the average cputime needed for determining a single moment γ_k, for $N = 50$, using respectively the triangulation approach and Gauss-Green theorem in polar coordinates.

The results are obtained by running our codes in Matlab R2018a, on a 2,7GHz Intel Core i5 CPU with 16 GB of RAM. The `polyshape` Matlab built-in environment is used to treat the polygonal regions, since it is able to manage even very complicated instances (regions defined by finite union, intersection, set difference of polygons, along with their triangulations).

We observe that since the rules in [1] require a huge number of nodes, the quantities AE and RE provide only estimates of the quality of the moment approximation. Both the approaches are very fast, the procedure based on Gauss-Green theorem being generally more rapid, though sometimes seems less precise (at least in our implementation). Furthermore, Gaussians are usually a little slower, since the first strategy requires the numerical evaluation of the T-Owen function, while the second one needs the fast computation of some one dimensional integrals.

Concerning numerical integration on scattered data, in Section 2 we have shown that the cubature weights $w_i = W_i$, $i = 1, \ldots, N$, can be obtained by
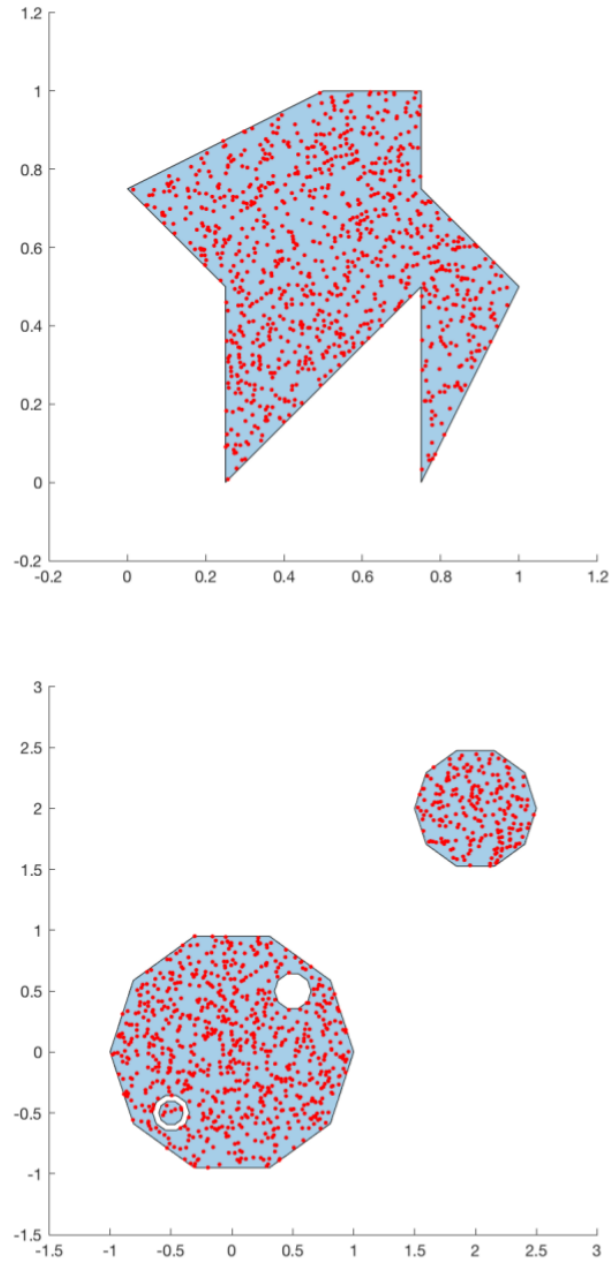
Figure 6: The polygonal regions (cyan) Ω_1 (top) and Ω_2 (bottom) with scattered points (red).

		MQ	G	IMQ	W2	TPS	RP
Ω_1	AE	$4e-15$	$3e-15$	$4e-15$	$3e-15$	$2e-13$	$1e-15$
	RE	$7e-15$	$7e-15$	$9e-15$	$2e-14$	$3e-12$	$2e-14$
	CPU	$1e-03$	$1e-03$	$1e-03$	$5e-04$	$5e-04$	$6e-04$
Ω_2	AE	$7e-14$	$2e-14$	$3e-14$	$8e-14$	$3e-12$	$1e-12$
	RE	$1e-14$	$1e-14$	$1e-14$	$2e-13$	$6e-13$	$2e-14$
	CPU	$7e-03$	$8e-03$	$8e-03$	$4e-03$	$4e-03$	$5e-03$

Table 1: Max *estimated* absolute and relative moment errors (respectively AE, RE) and average cputime CPU needed for determining a single moment γ_k, over Ω_1, Ω_2, by the triangulation approach.

		MQ	G	IMQ	W2	TPS	RP
Ω_1	AE	$2e-14$	$2e-14$	$5e-13$	$8e-15$	$9e-15$	$3e-15$
	RE	$4e-14$	$5e-14$	$1e-12$	$5e-14$	$2e-13$	$4e-14$
	CPU	$6e-05$	$3e-04$	$8e-05$	$1e-04$	$6e-05$	$4e-05$
Ω_2	AE	$3e-12$	$1e-13$	$5e-13$	$2e-14$	$7e-12$	$2e-11$
	RE	$3e-13$	$2e-13$	$3e-13$	$6e-14$	$3e-13$	$3e-13$
	CPU	$2e-04$	$2e-03$	$5e-04$	$4e-04$	$2e-04$	$2e-04$

Table 2: Max *estimated* absolute and relative moment errors (respectively AE, RE) and average cputime CPU needed for determining a single moment γ_k, over Ω_1, Ω_2, by Gauss-Green approach in polar coordinates.

solving a linear system $\mathcal{A}\mathbf{W} = \mathbf{I}$ where $\mathcal{A}$ is the interpolation matrix and $\mathbf{I}$ the possibly augmented vector of the moments. Unfortunately, depending on the pointset and on the RBF, $\mathcal{A}$ can be severely ill conditioned and small errors in the vector $\mathbf{I}$ may doom to failure the determination of $\mathbf{W}$. Keeping this in mind, we approximated numerically

$$\int_{\Omega_s} f(x,y)\, dx\, dy \approx \sum_{i=1}^{N} w_i f(x_i, y_i)$$

where $P_i = (x_i, y_i) \in \Omega_s$, $i = 1, \ldots, N$ are the scattered points, and w_i the weights obtained by the aforemented procedure, solving the moment matching system $\mathcal{A}\mathbf{W} = \mathbf{I}$ by Matlab backslash (i.e. by the so called *direct approach*). All the RBF moments are computed applying Gauss-Green theorem in polar coordinates.

19

In particular, we considered the following test functions

$$f_1(x, y) = \exp(x - y), \tag{20}$$
$$f_2(x, y) = \exp(5(x - y)), \tag{21}$$
$$f_3(x, y) = \sqrt{(x - 0.3)^2 + (y - 0.3)^2}. \tag{22}$$

Observe that f_1 and f_2 are smooth (indeed analytic) functions (with f_2 varying more rapidly), whereas f_3 has a singularity of the gradient in $(0.3, 0.3) \in \Omega_s$, for $s = 1, 2$.

Numerical results are displayed in Table 3, and show the good behaviour of W2, TPS, RP. We do not report the cubature errors obtained by means of Multiquadrics, Gaussian, Inverse Multiquadrics. In fact, in view of the extreme ill conditioning of the interpolation matrix $\mathcal{A}$, the direct method provides *impredictable* results when applied to these RBFs. With smooth RBFs alternative methods should be sought as is done with interpolation, but this will be a subject of further studies, since it is not clear how to easily extend the stabilized interpolation techniques to the cubature context.

The determination of the weights requires a cputime ranging from $0.04s$ when $N = 200$ to $0.1s$ when $N = 800$.

| | N | Ω_1 | | | Ω_2 | | |
		W2	TPS	RP	W2	TPS	RP
	200	$2e-03$	$4e-04$	$1e-04$	$1e-02$	$6e-04$	$2e-04$
f_1	400	$2e-04$	$3e-05$	$1e-05$	$1e-03$	$2e-04$	$2e-05$
	800	$5e-05$	$2e-05$	$5e-06$	$4e-04$	$3e-05$	$4e-06$
	200	$2e-02$	$2e-02$	$9e-03$	$6e-02$	$5e-03$	$9e-04$
f_2	400	$2e-03$	$4e-03$	$3e-03$	$1e-03$	$2e-04$	$2e-05$
	800	$1e-03$	$2e-03$	$7e-04$	$2e-03$	$1e-03$	$3e-04$
	200	$1e-03$	$8e-04$	$1e-05$	$9e-03$	$2e-04$	$2e-04$
f_3	400	$2e-04$	$2e-04$	$5e-05$	$2e-03$	$1e-04$	$9e-05$
	800	$2e-05$	$7e-07$	$9e-06$	$4e-04$	$1e-05$	$2e-07$

Table 3: Max *estimated* cubature relative errors on computing $\int_{\Omega_s} f_j(x, y) \, dx \, dy$ with $j = 1, 2, 3$, $s = 1, 2$ by the procedure using Gauss-Green approach in polar coordinates, for Wendland W2, Thin-Plate Splines (TPS), Radial Powers r^3 (RP).

Finally in Table 4, we display the ratio

$$1 \leq \sigma := \frac{\sum_{i=1}^{N} |\tilde{w}_i|}{\left| \sum_{i=1}^{N} \tilde{w}_i \right|} \approx \frac{\sum_{i=1}^{N} |\tilde{w}_i|}{area(\Omega)} \tag{23}$$

as a stability index of the cubature rule (a familiar concept in the framework of algebraic quadrature/cubature). Indeed, by (9) the 1-norm of the computed weights, $\|\tilde{\mathbf{w}}\|_1 = \sum_{i=1}^{N} |\tilde{w}_i|$, measures the effect of perturbations on the functional data, while the ratio σ attains its minimal value 1 for all positive weights.

We observe that in all the experiments, the rules had some negative weights, though few and of small magnitude, so that σ remains bounded below 2 (in particular with TPS it tends to stay close to 1). The numerical results say again that our scattered cubature rules on polygonal domains by RBFs of finite regularity, can be safely used even when noisy function evaluations are available.

	Ω_1			Ω_2		
N	W2	TPS	RP	W2	TPS	RP
200	1.44	1.10	1.48	1.68	1.18	1.74
400	1.62	1.30	1.62	1.37	1.09	1.43
800	1.38	1.10	1.38	1.51	1.12	1.54

Table 4: The stability index σ in (23) on the domains Ω_1, Ω_2.

References

[1] B. Bauman, A. Sommariva, M. Vianello, Compressed cubature over polygons with applications to optical design, J. Comput. Appl. Math. 370 (2020).

[2] M.D. Buhmann, Radial Basis Functions: Theory and Implementations, Cambridge University Press, 2003.

[3] R. Cavoretto, A. De Rossi and E. Perracchione, Optimal selection of local approximants in RBF-PU interpolation, J. Sci. Comput. 74 (2018), 1–22.

[4] R. Cavoretto, A. De Rossi, M.S. Mukhametzhanov and Ya.D. Sergeyev, On the search of the shape parameter in radial basis functions using univariate global optimization methods, J. Glob. Optim., published online 5 November 2019.

[5] G.E. Fasshauer, Meshfree Approximation Methods with Matlab, World Scientific Publishers, 2007.

[6] G.E. Fasshauer and M. Mc Court, Kernel-based Approximation Methods using Matlab, World Scientific Publishers, 2015.

[7] G.E. Fasshauer and J.G. Zhang, On choosing "optimal" shape parameters for RBF approximation, Numer. Algorithms 45 (2007), 345–368.

[8] B. Fornberg and N. Flyer, Solving PDEs with radial basis functions, Acta Numer. 24 (2015), 215–258.

[9] B. Fornberg and E. Larsson, Theoretical and computational aspects of multivariate interpolation with increasingly flat radial basis functions, Comput. Math. Appl. 49 (2005), 103–130.

[10] B. Fornberg, E. Larsson and N. Flyer, Stable computations with Gaussian radial basis functions, SIAM J. Sci. Comput. 33 (2011), 869–892.

[11] Mathworks, Polyshape function documentation, `www.mathworks.com/help/matlab/ref/polyshape.html`.

[12] J.A. Reeger and B. Fornberg, Numerical quadrature over smooth surfaces with boundaries, J. Comput. Phys. 355 (2018), 176–190.

[13] R. Schaback, Error estimates and condition numbers for radial basis function interpolation, Adv. Comput. Math. 3 (1995), 251-264.

[14] A. Sommariva, Numerical software page, `www.math.unipd.it/~alvise/software.html`.

[15] A. Sommariva, M. Vianello, Numerical cubature on scattered data by Radial Basis Functions, Computing 76 (2006), 295–310.

[16] A. Sommariva, M. Vianello, Meshless cubature by Green's formula, Appl. Math. Comput. 183 (2006), 1098–1107.

[17] H. Wendland, Scattered Data Approximation, Cambridge University Press, 2005.

[18] WolframAlpha, Online Integral Calculator, `www.wolframalpha.com/calculators/integral-calculator`

5 Appendix

We list below some of the primitives that we have computed via Wolfram Alpha, in the context of Gauss-Green approach in polar coordinates, distinguishing the cases in view of the RBF support.

5.1 Radial Basis Functions having $[0, \infty)$ as support

Given a RBF ϕ having $\mathbb{R}^+$ as support, we compute first

$$\Psi(\rho) := \int_0^\rho \phi(r) r \, dr$$

and then determine by [18] a primitive $\mathcal{P}_c$ of

$$\int \Psi(c/\sin(s)) \, ds.$$

We point out that for those RBF in which we were not available to compute $\mathcal{P}_c$, the cubature results can be achieved by means of adaptive quadrature or selected high order (shifted) gaussian rules.

Using symbolic-calculus we obtained

- if ϕ is the Multiquadric, i.e. $\phi(r) = \sqrt{1 + r^2}$ then

$$\mathcal{P}_c(s) = \frac{1}{3} \left(\frac{c^2 \sin(s) \cos(s) \left(c^2 \csc^2(s) + 1\right)^{3/2}}{-2c^2 + \cos(2s) - 1} - \frac{\sqrt{2} \sin^3(s) \left(c^2 \csc^2(s) + 1\right)^{3/2}}{\sqrt{-c^2} \left(-2c^2 + \cos(2s) - 1\right)^{3/2}} \right.$$
$$\left(2\sqrt{-c^2} \log\left(\sqrt{-2c^2 + \cos(2s) - 1} + \sqrt{2} \cos(s)\right) + \right.$$
$$\left. \left(c^2 + 3\right) c^2 \tanh^{-1}\left(\frac{\sqrt{2}\sqrt{-c^2} \cos(s)}{\sqrt{-2c^2 + \cos(2s) - 1}}\right)\right) - s \right);$$

- if ϕ is the Inverse Multiquadric, i.e. $\phi(r) = \frac{1}{\sqrt{1+r^2}}$ then

$$\mathcal{P}_c(s) = \frac{\sqrt{2} \sin(s) \sqrt{c^2 \csc^2(s) + 1} \log\left(\sqrt{-2c^2 + \cos(2s) - 1} + \sqrt{2} \cos(s)\right)}{\sqrt{-2c^2 + \cos(2s) - 1}}$$
$$- \frac{\sqrt{2}\sqrt{-c^2} \sin(s) \sqrt{c^2 \csc^2(s) + 1} \tanh^{-1}\left(\frac{\sqrt{2}\sqrt{-c^2} \cos(s)}{\sqrt{-2c^2 + \cos(2s) - 1}}\right)}{\sqrt{-2c^2 + \cos(2s) - 1}} - s;$$

- if ϕ is the Thin-Plate Spline, i.e. $\phi(r) = r^2 \log(r)$ then

$$\mathcal{P}_c(s) = \frac{c^4 s}{6} + \frac{13}{72} c^4 \cot(s) + \frac{7}{144} c^4 \cot(s) \csc^2(s)$$
$$+ \frac{1}{12} c^4 (\cos(2s) - 2) \cot(s) \csc^2(s) \log(c \csc(s));$$

- if ϕ is the cubic Radial Power, i.e. $\phi(r) = r^3$ then

$$\mathcal{P}_c(s) \frac{1}{5} c^5 \left(-\frac{1}{64} \csc^4(s/2) - \frac{3}{32} \csc^2(s/2) + \frac{1}{64} \sec^4(s/2) + \frac{3}{32} \sec^2(s/2)\right.$$
$$\left. + \frac{3}{8} \log\left(\sin(s/2)\right) - \frac{3}{8} \log\left(\cos(s/2)\right)\right);$$

23

- if ϕ is the quintic Radial Power, i.e. $\phi(r) = r^5$ then

$$\mathcal{P}_c(s) = \frac{1}{7}c^7 \left(-\frac{1}{384}\csc^6(s/2) - \frac{1}{64}\csc^4(s/2) - \frac{5}{64}\csc^2(s/2) + \frac{1}{384}\sec^6(s/2) + \right.$$
$$\left. \frac{1}{64}\sec^4(s/2) + \frac{5}{64}\sec^2(s/2) + \frac{5}{16}\log\left(\sin(s/2)\right) - \frac{5}{16}\log\left(\cos(s/2)\right) \right);$$

- if ϕ is the Radial Power $\phi(r) = r^7$ then

$$\mathcal{P}_c(s) = \frac{1}{9}c^9 \left(-\frac{\csc^8(s/2)}{2048} - \frac{5\csc^6(s/2)}{1536} - \frac{15\csc^4(s/2)}{1024} - \frac{35}{512}\csc^2(s/2) + \right.$$
$$\frac{\sec^8(s/2)}{2048} + \frac{5\sec^6(s/2)}{1536} + \frac{15\sec^4(s/2)}{1024} + \frac{35}{512}\sec^2(s/2) + $$
$$\left. \frac{35}{128}\log\left(\sin(s/2)\right) - \frac{35}{128}\log\left(\cos(s/2)\right) \right); \tag{24}$$

- if ϕ is the Gaussian $\phi(r) = \exp\left(-r^2\right)$ then

$$\Psi(\rho) := \int_0^\rho r\phi(r)\,dr = -\frac{\exp\left(-\rho^2\right) - 1}{2},$$

but we are not able to get a closed form of $\mathcal{P}_c$, i.e. to compute explicitly $\int \Psi(c/\sin(s))\,ds$;

- if ϕ is the Matérn $\phi(r) = \exp\left(-r\right)$ then

$$\Psi(\rho) := \int_0^\rho r\phi(r)\,dr = 1 - (1 + r)\exp(-r)$$

but we are not able to get a closed form of $\mathcal{P}_c$, i.e. to compute explicitly $\int \Psi(c/\sin(s))\,ds$;

- if ϕ is the Matérn $\phi(r) = (1 + r)\exp\left(-r\right)$ then

$$\Psi(\rho) := \int_0^\rho r\phi(r)\,dr = 3 - (3 + 3r + r^2)\exp(-r)$$

but we are not able to get a closed form of $\mathcal{P}_c$, i.e. to compute explicitly $\int \Psi(c/\sin(s))\,ds$.

5.2 Radial Basis Functions having $[0, 1]$ as support

In the description of the Gauss-Green approach in polar coordinates, we have shown that compactly supported RBF need some further care. In the next analysis we suppose that their support is $[0, 1]$.

If $\phi(r) = (g(r))_+ = \max(g(r), 0)$, we first compute

$$\psi(\rho) = \int_0^\rho r g(r) dr$$

and then a primitive $\mathcal{P}_c^*$ of

$$\int \psi(c/\sin(s)) \, ds.$$

Once $\mathcal{P}_c^*$ is at hand, we easily achieve the integrals required by the Gauss-Green theorem in polar coordinates. Here we list $\mathcal{P}_c^*$ some Wendland RBF, i.e. the so called W0, W2, W4, W6.

- If ϕ is the Wendland W0 RBF, i.e.

$$\phi(r) = (\max(0, (1 - r)))^2 = (1 - r)_+^2$$

  then

$$\mathcal{P}_c^*(s) = \frac{1}{20} c^5 \csc^4(s) - \frac{1}{6} c^4 \csc^3(s) + \frac{1}{6} c^3 \csc^2(s) \qquad (25)$$

- If ϕ is the Wendland W2 RBF, i.e.

$$\phi(r) = (1 + 4r) \cdot (1 - r)_+^4 = (1 + 4r) \cdot (\max(0, (1 - r)))^4$$

  then

$$
\begin{aligned}
\mathcal{P}_c^*(s) = & -\frac{1}{672} c^7 \csc^6(s/2) - \frac{1}{112} c^7 \csc^4(s/2) - \frac{5}{112} c^7 \csc^2(s/2) + \\
& \frac{1}{672} c^7 \sec^6(s/2) + \frac{1}{112} c^7 \sec^4(s/2) + \frac{5}{112} c^7 \sec^2(s/2) + \\
& \frac{5}{28} c^7 \log(\sin(s/2)) - \frac{5}{28} c^7 \log(\cos(s/2)) + \frac{4}{3} c^6 \cot(s) + \\
& \frac{1}{2} c^6 \cot(s) \csc^4(s) + \frac{2}{3} c^6 \cot(s) \csc^2(s) - \frac{1}{16} c^5 \csc^4(s/2) - \\
& \frac{3}{8} c^5 \csc^2(s/2) + \frac{1}{16} c^5 \sec^4(s/2) + \frac{3}{8} c^5 \sec^2(s/2) + \frac{3}{2} c^5 \log(\sin(s/2)) - \\
& \frac{3}{2} c^5 \log(\cos(s/2)) + \frac{5}{3} c^4 \cot(s) + \frac{5}{6} c^4 \cot(s) \csc^2(s) - \frac{1}{2} c^2 \cot(s);
\end{aligned}
$$

- If ϕ is the Wendland W4 RBF, i.e.

$$\phi(r) = (35r^2 + 18r + 3)(1 - r)_+^6 = (35r^2 + 18r + 3)(\max(0, (1 - r)))^6$$

then

$$\mathcal{P}_c^*(s) = -\frac{64}{45}c^{10}\cot(s) - \frac{7}{18}c^{10}\cot(s)\csc^8(s) - \frac{4}{9}c^{10}\cot(s)\csc^6(s) -$$

$$\frac{8}{15}c^{10}\cot(s)\csc^4(s) - \frac{32}{45}c^{10}\cot(s)\csc^2(s) + \frac{1}{96}c^9\csc^8(s/2) +$$

$$\frac{5}{72}c^9\csc^6(s/2) + \frac{5}{16}c^9\csc^4(s/2) + \frac{35}{24}c^9\csc^2(s/2) - \frac{1}{96}c^9\sec^8(s/2) -$$

$$\frac{5}{72}c^9\sec^6(s/2) - \frac{5}{16}c^9\sec^4(s/2) - \frac{35}{24}c^9\sec^2(s/2) - \frac{35}{6}c^9\log(\sin(s/2)) +$$

$$\frac{35}{6}c^9\log(\cos(s/2)) - 24c^8\cot(s) - \frac{15}{2}c^8\cot(s)\csc^6(s) - 9c^8\cot(s)\csc^4(s) -$$

$$12c^8\cot(s)\csc^2(s) + \frac{1}{6}c^7\csc^6(s/2) + c^7\csc^4(s/2) + 5c^7\csc^2(s/2) -$$

$$\frac{1}{6}c^7\sec^6(s/2) - c^7\sec^4(s/2) - 5c^7\sec^2(s/2) - 20c^7\log(\sin(s/2)) +$$

$$20c^7\log(\cos(s/2)) - \frac{56}{3}c^6\cot(s) - 7c^6\cot(s)\csc^4(s) - \frac{28}{3}c^6\cot(s)\csc^2(s) +$$

$$\frac{14}{3}c^4\cot(s) + \frac{7}{3}c^4\cot(s)\csc^2(s) - \frac{3}{2}c^2\cot(s).$$

- If ϕ is the Wendland W6 RBF, i.e.

$$\phi(r) = (32r^3 + 25r^2 + 8r + 1)(\max(0, (1 - r)))^8$$

26

then

$$
\begin{aligned}
\mathcal{P}_c^*(s) = & -\frac{c^{13}\csc^{12}(s/2)}{19968} - \frac{7c^{13}\csc^{10}(s/2)}{16640} - \frac{7c^{13}\csc^{8}(s/2)}{3328} - \frac{7}{832}c^{13}\csc^{6}(s/2)- \\
& \frac{105c^{13}\csc^{4}(s/2)}{3328} - \frac{231c^{13}\csc^{2}(s/2)}{1664} + \frac{c^{13}\sec^{12}(s/2)}{19968} + \frac{7c^{13}\sec^{10}(s/2)}{16640}+ \\
& \frac{7c^{13}\sec^{8}(s/2)}{3328} + \frac{7}{832}c^{13}\sec^{6}(s/2) + \frac{105c^{13}\sec^{4}(s/2)}{3328} + \frac{231c^{13}\sec^{2}(s/2)}{1664}+ \\
& \frac{231}{416}c^{13}\log\left(\sin(s/2)\right) - \frac{231}{416}c^{13}\log\left(\cos(s/2)\right) + \frac{64}{9}c^{12}\cot(s)+ \\
& \frac{7}{4}c^{12}\cot(s)\csc^{10}(s) + \frac{35}{18}c^{12}\cot(s)\csc^{8}(s) + \frac{20}{9}c^{12}\cot(s)\csc^{6}(s)+ \\
& \frac{8}{3}c^{12}\cot(s)\csc^{4}(s) + \frac{32}{9}c^{12}\cot(s)\csc^{2}(s) - \frac{1}{160}c^{11}\csc^{10}(s/2)- \\
& \frac{3}{64}c^{11}\csc^{8}(s/2) - \frac{7}{32}c^{11}\csc^{6}(s/2) - \frac{7}{8}c^{11}\csc^{4}(s/2) - \frac{63}{16}c^{11}\csc^{2}(s/2)+ \\
& \frac{1}{160}c^{11}\sec^{10}(s/2) + \frac{3}{64}c^{11}\sec^{8}(s/2) + \frac{7}{32}c^{11}\sec^{6}(s/2)+ \\
& \frac{7}{8}c^{11}\sec^{4}(s/2) + \frac{63}{16}c^{11}\sec^{2}(s/2) + \frac{63}{4}c^{11}\log(\sin(s/2))- \\
& \frac{63}{4}c^{11}\log(\cos(s/2)) + \frac{704}{15}c^{10}\cot(s) + \frac{77}{6}c^{10}\cot(s)\csc^{8}(s)+ \\
& \frac{44}{3}c^{10}\cot(s)\csc^{6}(s) + \frac{88}{5}c^{10}\cot(s)\csc^{4}(s) + \frac{352}{15}c^{10}\cot(s)\csc^{2}(s)- \\
& \frac{11}{192}c^{9}\csc^{8}(s/2) - \frac{55}{144}c^{9}\csc^{6}(s/2) - \frac{55}{32}c^{9}\csc^{4}(s/2) - \frac{385}{48}c^{9}\csc^{2}(s/2)+ \\
& \frac{11}{192}c^{9}\sec^{8}(s/2) + \frac{55}{144}c^{9}\sec^{6}(s/2) + \frac{55}{32}c^{9}\sec^{4}(s/2) + \frac{385}{48}c^{9}\sec^{2}(s/2)+ \\
& \frac{385}{12}c^{9}\log(\sin(s/2)) - \frac{385}{12}c^{9}\log(\cos(s/2)) + \frac{132}{5}c^{8}\cot(s)+ \\
& \frac{33}{4}c^{8}\cot(s)\csc^{6}(s) + \frac{99}{10}c^{8}\cot(s)\csc^{4}(s) + \frac{66}{5}c^{8}\cot(s)\csc^{2}(s)- \\
& \frac{88}{15}c^{6}\cot(s) - \frac{11}{5}c^{6}\cot(s)\csc^{4}(s) - \frac{44}{15}c^{6}\cot(s)\csc^{2}(s)+ \\
& \frac{11}{6}c^{4}\cot(s) + \frac{11}{12}c^{4}\cot(s)\csc^{2}(s) - \frac{1}{2}c^{2}\cot(s)
\end{aligned}
$$

27